Advances in Science and Technology Research Journal

Advances in Science and Technology Research Journal, 2026, 20(7), 227–240
https://doi.org/10.12913/22998624/219279
ISSN 2299-8624, License CC-BY 4.0

Received: 2025.12.29
Accepted: 2026.05.15
Published: 2026.06.01

Dynamics of the response of a complex mathematical model of the human sense of vision to light signals

Ryszard Szczebiot[1], Leszek Gołdyn[1], Jakub Gajewski[2*], Roman Kaczyński[3], Aneta Wiktorzak[1]

[1] Faculty of Computer Science and Technology, University of Lomza, ul. Akademicka 14, 18-400 Lomza, Poland
[2] Faculty of Mechanical Engineering Department of Machine Design & Mechatronics, Lublin University of Technology, ul. Nadbystrzycka 36, 20-618 Lublin, Poland
[3] Faculty of Mechanical Engineering, Bialystok University of Technology, ul. Wiejska 45C, 15-351 Bialystok, Poland
* Corresponding author's e-mail: j.gajewski@pollub.pl

ABSTRACT

The paper presents a proposed solution for the dynamic response of a complex mathematical model of the human sense of vision to light signals. The solutions were based on the model proposed by authors. The solutions were independently developed for: the main path model, the feedback path model of the pupil's neuromotor system, and the solution combining the main path model with the feedback path model of the pupil's neuromotor system. Each of these solutions was developed for two cases. In the first case, the signal disturbing the human visual system was descriptively defined as a strong, short-term irritation of a light beam incident on the eyeball (a flash, represented in calculations by the Dirac function). The second case involved a situation of prolonged light beam incident on the eyeball of a not a moderate intensity (a unit step, represented in calculations by the Heaviside function). The solutions were given in the form of symbolic equations of the dynamic waveforms of the output signals and models with inserted parameter values. Based on these equations, graphs of the time courses of the output functions for light beam interference were constructed.

Keywords: human vision, mathematical model, automation system.

INTRODUCTION

The human sense of vision is one of the most important senses. Its proper operation, particularly in interaction with various devices and systems, is crucial. Mathematical modeling of human senses is crucial because it enables better integration of the automation system model with the human model interacting with it as an automation system. These models can then be combined to create a single, coherent, multi-circuit mathematical model of the automated system with signals affecting the human senses. Most biological processes exhibit pronounced nonlinearity in all its forms and combinations. Sensitivity threshold, saturation range, relay behavior, and hysteresis can be observed. These factors describe behavior in steady, static, and normalized states. Analyzing the dynamic time course of human behavior observed in response to external stimuli, one can observe interactions defined in automation as overshoot or higher-order inertial reactions.

A wide variety of works have been published on algorithms utilizing the modes of the human visual system. Daley [1], based on the Georgia Tech Vision model, proposed algorithms for the modes of the human visual system. Thomas [2] studied input-output models representing steady-state vision in humans. Based on the properties of the human visual system, Matsui [3] proposed a non-stationary spatiotemporal model of human vision. Research on this topic has also been conducted. For example, Karmakara [4] studied the assessment of a jet pilot's vision in a virtual

environment. This study aimed to investigate how effective vision analysis tools included in digital human modeling software could be.

Authors [5] describe a real-time computer vision and machine learning system for modeling and recognizing human behaviors in a visual surveillance task. Samma [6] proposed created SqueezeNet, an alternative compressed and diminutive network and was trained to recognize objects as a broad classification system. The paper [7] presents a deep learning-based human height estimation approach using a stereo vision system. Rashdi [8] presents a study on optimizing light spectra for enhancing the contrast between two objects in visual inspection systems.

The paper [9] proposes an artificial vision architecture consisting of spiking photodetectors and artificial synapses, closely mirroring the intricacies of the human visual system. In the paper [10] authors proposed a simple and effective full-reference color image quality measure (CQM) based on reversible luminance and chrominance (YUV) color transformation and peak signal-to-noise ratio (PSNR) measure. Hoshino [11] proposed a robot vision system in which original images captured by a camera sensor are described by the optical flow and are then used as inputs for the human and action classifications. The paper [12] use human-computer interaction and computer vision technology to solve the existing problems of intelligent vehicle violation detection systems. Artificial vision with finely resolved polychromatic artificial cone cells are demonstrated surpassing human vision using visible multispectral camera was proposed [13].

Hoshino [14] proposed a robot vision system in which images described by the optical system are used as an input for the classification of humans and actions in the input images. The study [15] provides an overview of the existing computational image generation techniques that properly simulate human vision in the presence of wave front aberrations. Bochen [16] explores the application of the vision system in the robot and its ability in object detection in collaborative with humans. The paper [17] develops a visual system for human-robot interaction, including face detection, face location, gender recognition, facial expression recognition and reproduction. Oda [18] presents a system development of biped walking robot control cooperating with human visual motion. The paper [19] deals with a novel approach for the identification of human and robot collision based on vision systems. Pladere [20] presents the need for understanding, assessing, and correcting common eye and vision problems to increase inclusivity to help broaden a responsible uptake of XR HMDs. In the study [21] authors present a robot which is equipped with an image-sensing device human vision component that acquires the age, gender, and direction of the face.

Branson [22] present a visual recognition system for fine-grained visual categorization. Piroddi [23] presents the case of reverse engineering the human vision system. The paper [24] presents a mobile system for pedestrian detection in severe lighting conditions. The paper [25] describes development and testing of a novel peripheral–central vision system to detect, localize, and classify an airborne threat. In the paper [26] authors designed an advanced active vision system for humanoid robots that imitates human eye movements.

Tran [27] presents research studies the characteristics of human vision perception. The paper [28] presents a dual-loop implementation architecture that enables a robot vision system to learn from human vision in disassembly tasks. Gong [29] presents memristor-based reservoir computing system with integrated sensing and memory functions provides a solution to effectively improve the computational efficiency of artificial vision networks. The paper [30] discusses an AI based vision system that is responsible for the evaluation of an assembly performed in the context of a hybrid manufacturing system. Al-Rashdi [31] presents a study on optimizing light spectra for enhancing the contrast between two objects in visual inspection systems.

The sense of vision is one of the most important human senses. Its correct operation, especially when interacting with various devices and systems, is functionally very important. Correct mathematical modeling of a human sense (e.g., the sense of sight) enables better integration with the automation system, creating a coherent, superior system. It is then possible to combine several models and build a single, coherent, multi-circuit automation system that interacts with and interacts with the human senses.

Few scientific works treat humans as complex automation systems. For example, in his book, Antoniewicz [32] proposed a simplified model of the primary human visual system, excluding the defensive protection pathways and without

a model of defensive reactions. For a long time, there had been no proposals for such a model or its development in the literature. Only after many years, in paper [33], the authors took up this topic and proposed an extended mathematical model of an automatic system of human eye reaction to a forcing light pulse. A block diagram of the proposed system with five human reaction paths is given (Figure 1).

The model of the human visual system proposed in [33] is very complex. The system has several feedback paths responsible for protective functions in the human vision process. It consists of a large number of gain coefficients, transport delay times, and time constants related to the inertia of the action. Furthermore, the transport delay times occur in various locations within the system and vary in value. Given this model's complexity, determining the dynamic characteristics of the human response signals to various light stimuli is very complex and requires many difficult and labor-intensive calculations.

DYNAMICS OF THE REACTION OF A COMPLEX MODEL OF HUMAN VISION TO LIGHT SIGNALS

Solution methodology of a complex model of human vision to light signals

The model proposed in [33], along with a block diagram of a system related to the dynamic process of human vision and its defensive reactions in the event of disruptive disturbances (Figure 1), represents a self-protection process, self-regulation to reduce the impact of disturbances, or a process of adaptation of the visual system to the prevailing situation. This model represents a complex multi-path system with a large number of amplification factors, transport and inertial delay times. Each block diagram and its elements can be represented and described in various domains, for example, in time, frequency, or algebra. Transitioning from one domain to another is not always a simple process, especially if the presented system is a complex, multi-path system with a large number of functional parameters. The process of solving a modeling system representing the dynamic waveforms of its output signals in response to excitation (disturbance) is very complex and in many cases requires difficult and labor-intensive calculations.

In the paper, based on the proposed model [33], the following solutions were developed: an independent model of the main track, a model of the feedback track of the pupil's neuromotor system, and a solution combining the main track model with the feedback track of the pupil's neuromotor system. The block diagram of this model is shown in Figure 2.

Each of these solutions was tested for two scenarios. In the first case, the signal disturbing the human visual system was described as a strong but short-lived irritation from a beam of

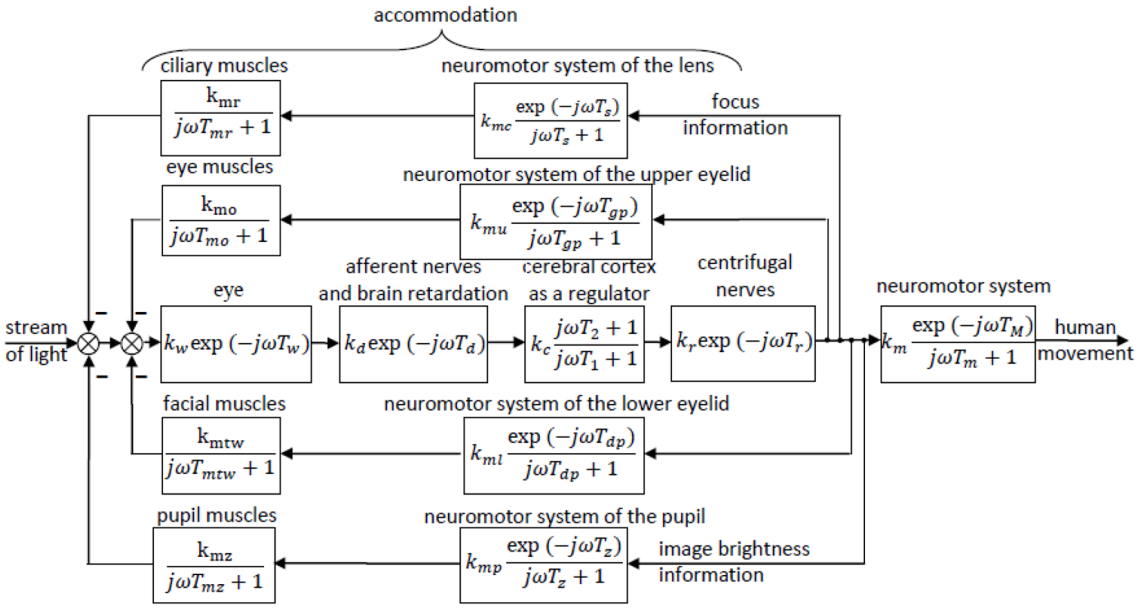

Figure 1. Detailed block diagram of the light excitation system for human reaction [33]

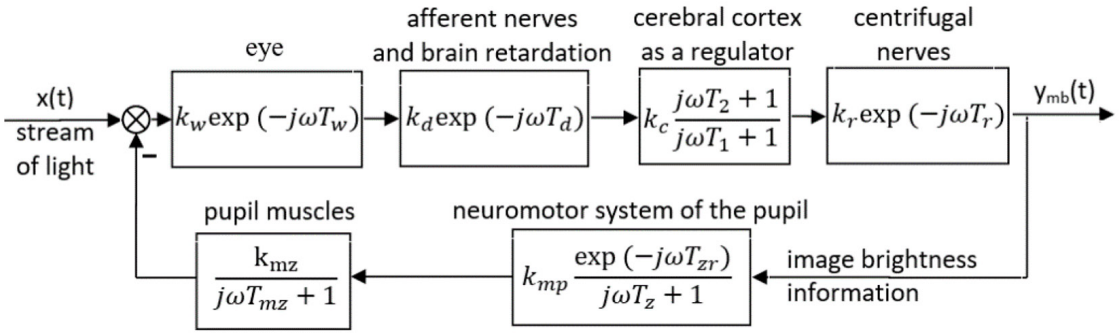

Figure 2. Block diagram of the eye response of the main and negative feedback pathways of the pupillary neuromotor system

light falling on the eyeball (a flash). The second case could refer to a situation where a beam of light falls on the eyeball for a prolonged period, at a moderate intensity, but still a moderate (unit jump).

In the paper, standard interference signals of flash represented in the modeling as Dirac functions were used to solve the studied models:

$$x(t) = s(t) = \{0 \text{ for } t < 0, \\ \infty \text{ for } t = 0,\ 0 \text{ for } t > 0\}. \quad (1)$$

and the unit jump signal represented in the modeling as a Heaviside function:

$$x(t) = 1 \quad (2)$$

In practical calculations, the Laplace transforms of these functions were used. Correspondingly, for the Dirac function (1), the transform equation has the form:

$$X(s) = 1, \quad (3)$$

and for the Heaviside function (2) the transform equation has the form:

$$X(s) = 1/s. \quad (4)$$

In this work, the diagram (Figure 2) shows the main path of the control system consisting of blocks representing important elements of the eye-brain system [33]:

$$G_m(s) = \frac{k_w e^{-T_w s} k_d e^{-T_d s} k_c}{(T_2 s + 1) e^{-T_r s} k_r} \quad (5)$$
$$T_1 s + 1$$

where: k_w – eye amplification factor (overall); T_w – transport delay time (related directly to the eye); k_d – afferent nerve (optical nerve) gain factor; T_d – transport delay time related to the transmission of a signal stimulated by the afferent nerve and brain reaction time; k_c – gain factor of the central part of the nervous system (cerebral cortex); T_2 – lead time related to the self-adjusting regulatory action of the central part of the nervous system; T_r – transport delay time (signal transmission) of the centrifugal nerve; k_r – centrifugal (motor) nerve gain factor; T_1 – time constant of inertia associated with the central part of the nervous system.

The mathematical model of the main circuit is presented in an algebraic form, i.e., in the form of the operator transfer function $G_m(s)$ (5). Using the properties of the operator calculus, the equation of the output signal transform was determined:

$$Y_m(s) = G_m(s)X(s) = \\ \frac{k_w e^{-T_w s} k_d e^{-T_d s} k_c}{(T_2 s + 1) e^{-T_r s} k_r} X(s) \quad (6)$$
$$= \frac{}{T_1 s + 1}$$

where: $X(s)$ is the Laplace transform of the input signal to the main path.

Determining the dynamic properties of the main circuit required solving Equation 6 for the assumed disturbances.

Solutions and discussion of results of a complex model of human vision to light signals. The transformations and calculations in this work were performed using the Mathematica package [34]. In the case of disturbance using the Dirac function (1), a symbolic solution was obtained for the dynamic waveform of the main circuit's output signal:

$$y_{mD}(t) = k_c k_d k_r k_w \left(\frac{e^{-t+T_d+T_r+T_w} HeavisideTheta [t - T_d - T_r - T_w]}{T_1} + HeavisideTheta [t - T_d - T_r - T_w] \left(\frac{-\frac{e^{-t+T_d+T_r+T_w}}{T_1}}{T_1^2} + DiracDelta [t - T_d - T_r - T_w] \right) T_2 \right) \quad (7)$$

In the case of disturbance by the Heaviside function (2), the symbolic solution of the dynamic waveform of the output signal of the main path has the form:

$$y_{mH}(t) = \frac{1}{T_1} e^{\frac{-t}{T_1}} HeavisideTheta [t - T_d - T_r - T_w] k_c k_d k_r k_w \left(\left(e^{\frac{t}{T_1}} - e^{\frac{T_d+T_r+T_w}{T_1}} \right) T_1 + e^{\frac{T_d+T_r+T_w}{T_1}} T_2 \right) \quad (8)$$

The determined dynamic waveform functions of the main path signals, in symbolic forms (7) and (8), describe human responses to a moderate light interference. Determining the dynamic waveform responses graphically in the adopted model (5) requires selecting the model parameter values, i.e., the amplification coefficients, transport delay times, and time constants.

Symbolic equations describe general models of phenomena and systems, in this case, a model of human vision to light signals. Checking the effectiveness of the model requires inserting the parameter values of a specific example to obtain a parametric model. A parametric model, on the other hand, describes a specific example without providing the ability to examine the impact of parameters on the system's modeling accuracy.

Only partial parameter values of the proposed model can be found in the literature, and their sources are provided in the paper.

All signals in the model, in the actual eye-brain system, are neural signals with very low current intensity (in μA). This means that the signals cannot be amplified multiple times. In such a delicate system, there are no electric charge stores (accumulators). Amplification coefficients can be assumed to vary between 0.98 and 1. Values lower than 1 would be possible in the event of damage to any component of the system (e.g., due to disease or damage to any component). The amplification coefficients were assumed to be equal to unity [32]: k_w=1, k_c=1, k_d=1, k_r=1. These coefficients are dimensionless.

The main path model (5) also includes time parameters in the form of time constants and transport delay times. Delays associated with information transport via a current signal total approximately several hundredths of a second. Signal transmission distances are very small, but information transfer rates are also not very high. Modeling a signal with transport delay shifts the characteristic graph by the amount of the delay time. These times should not be neglected. However, a shifted graph on the time axis should be expected. Analyzing information from other sources, the following transport delay times were assumed for calculations [32]: T_w=0.07 [s], T_d=0.06 [s], T_r=0.02 [s].

The remaining time constants T_1 and T_2 included in model (5) refer to time constants describing the dynamics of brain function. Time constant T_1 refers to the inertial delay of brain function. Time constant T_2 is associated with the operation of every real device or mechanism. In practice, mechanisms operating without this time constant do not exist. In this work, T_1=0.05 [s]. T_2 is the lead time and is associated with a very small differential effect, resulting in very rapid operation. It can be assumed that the evolutionary process of human development has developed this brain function for protective purposes. However, in all systems, such an effect causes significant inertia and frequent overshoot. The lead time value T_2=0.0001 [s] was assumed.

Assuming the values of the described parameters of Equation 5, the dynamic course of the output function (7) for the Dirac function (1) takes the form:

$$y_{mD}(t) = 20.\, e^{20.(0.15-t)} HeavisideTheta [-0.15 + t] + 0.0001(-400.\, e^{20.(0.15-t)} + 20.\, DiracDelta[-0.15 + t]) HeavisideTheta[-0.15 + t] \quad (9)$$

The time graph of the output function of the main path $y_{mD}(t)$ (9) for the Dirac disturbance function is shown in Figure 3.

The time course of the eye-brain system's response to a short, disruptive light pulse, for the main model path only (Figure 2), is shown in Figure 3. The main path of the diagram does not account for the defensive actions modeled in the model's feedback loops. The time course is offset by the total transport delay time (T_d, T_r, T_w) associated with the passage of the interfering signal from the eye to the brain. This is illustrated by a rightward shift in the coordinate system. This phenomenon is present in the graph, but it must be analyzed for the eye-brain system due to the subtle visual process being studied. At this time, the brain does not yet react to the disruption because the disruptive signal has not yet reached the brain. In the model under study, the total delay time is the sum of the times $T_w+T_d+T_r$ and, for the assumed values, equals 0.15 s. After this time, information about the short-term, strong disruption triggers a rapid system response in the form of a strong current signal. The disturbing signal in the form of a Dirac function is very short and decays quickly. The brain's response (analyzing only the main path without any protective actions) represents the inertial decay of the signal to its initial pre-disturbance value. In automation, this corresponds to the differential action of the element. In the case of the obtained waveform, this takes approximately 0.2 s. This describes the lead time determined from the obtained waveform, which is 0.05 s.

Similarly, for the assumed parameters of equation (5), the dynamic course of the output function (8) for the Heaviside function (2) takes the form:

$$y_{mH}(t) = 20.e^{-20.t}$$
$$\left(0.002 + 0.05(-20.0855 + e^{20.t})\right) \quad (10)$$
$$HeavisideTheta[-0.15 + t]$$

The time graph of the output function of the main path $y_{mH}(t)$ (10) for the Heaviside disturbance function is shown in Figure 4.

The dynamic response shown in Figure 4 is the response of the main model path to a disturbance in the form of a Heaviside function. The response follows an inertial growth curve, offset by the transport delay associated with transmitting information to the brain. The response settling time does not follow a classic inertial curve due to the brain's preemptive action. The settling time for the assumed model parameter values is approximately 0.1 s, and the signal remains stable at its maximum value throughout the duration of the disturbing signal. This is consistent with the expected behavior of the human response to a continuous light signal that irritates the eye, in the absence of feedback that protects the eye and brain. It should be noted that in reality, the curves in Figure 3 and Figure 4 do not occur without protective feedback and are merely model curves.

The model presented in [32] has four feedback curves related to the protective actions of the sensors used and the main element in the main path, the cerebral cortex, as a regulator. In the initial phase of the system dynamics study, a single feedback path was selected, related to the influence of the transport delay of the pupillary neuromotor system (Figure 2). It consists of the

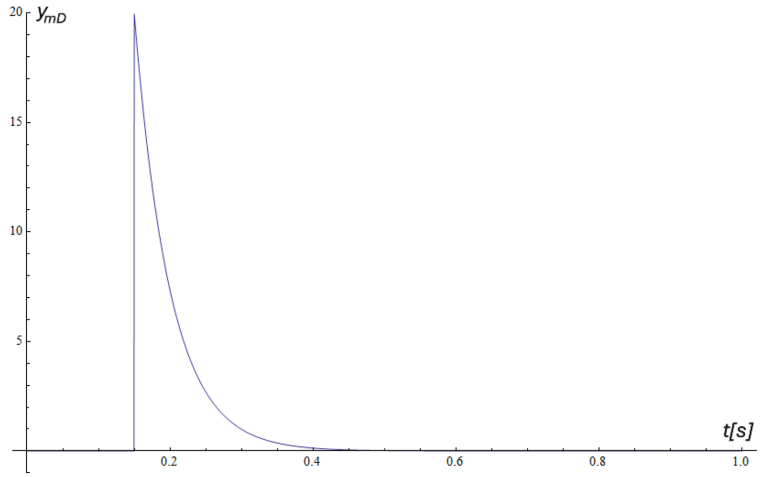

Figure 3. Time graph of the main path output function $y_{mD}(t)$ for the Dirac disturbance function.

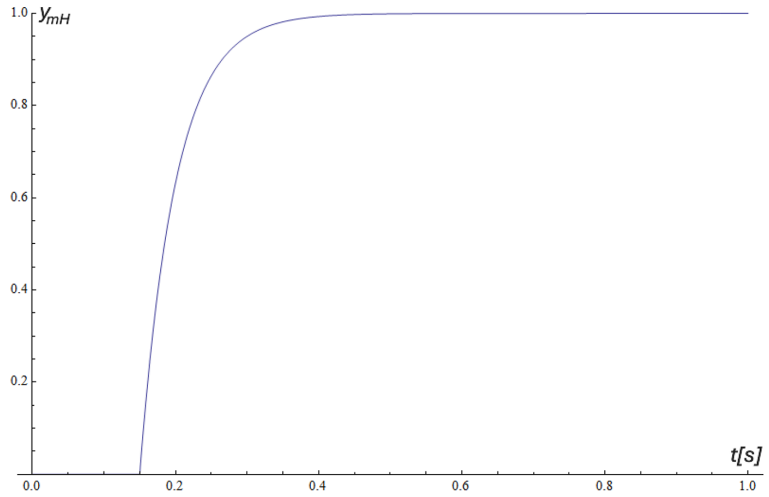

Figure 4. Time graph of the main path output function $y_{mH}(t)$ (10) for the Heaviside disturbance function

pupillary neuromotor system and the driving element of the pupillary muscles.

The mathematical model of the feedback path of the image brightness effect, in the form of an operator transfer function, is presented by the equation:

$$G_b(s) = k_{mp}\frac{e^{-T_{zr}s}}{T_z s + 1}k_{mz}\frac{1}{T_{mz}s + 1} \tag{11}$$

where: k_{mp} – amplification factor of the neuromuscular reaction system; T_{zr} – transport delay time of the pupil's neuromotor system; T_z – time constant related to the transport and inertial delay of the eye pupil; k_{mz} – coefficient of strengthening the pupillary muscles; T_{mz} – time constant of inertia of the action of the muscles of the pupil.

As a result of this path, a signal is generated that reduces the light flux incident on the eye, hence the negative feedback loop of the path. From the perspective of the automation system, this is a simplified model combining a first-order inertial term with a time constant T_z, amplified by the k_{mp} coefficient and a transport delay term with time T_z. The model of the pupillary muscle action is a first-order inertial term (time constant T_{mz}) and amplification coefficient k_{mz}. Consequently, the model presented in the analyzed path is a second-order inertial term with a transport delay and amplification.

From the feedback path model Equation 11, the equation for the transform of the output signal of the pupillary neuromotor feedback path $Y_b(s)$ was determined:

$$Y_b(s) = G_b(s)X(s) = \\ = k_{mp}\frac{e^{-T_{zr}s}}{T_z s + 1}k_{mz}\frac{1}{T_{mz}s + 1}X(s) \tag{12}$$

By introducing the Dirac disturbance transform function (3) into Equation 12, an algebraic model of the analyzed feedback path of the pupil's neuromotor system was obtained $Y_{bD}(s)$:

$$Y_{bD}(s) = k_{mp}\frac{e^{-T_{zr}s}}{T_z s + 1}k_{mz}\frac{1}{T_{mz}s + 1} \tag{13}$$

By introducing the Heaviside disturbance transform function (4) into Equation 12, an algebraic model of the feedback path of the pupil's neuromotor system was determined in the form of the equation $Y_{bH}(s)$:

$$Y_{bH}(s) = k_{mp}\frac{e^{-T_{zr}s}}{T_z s + 1}k_{mz}\frac{1}{T_{mz}s + 1}\frac{1}{s} \tag{14}$$

By solving models (13) and (14), we obtained symbolic dynamic waveforms of the output signals from the pupillary neuromotor feedback pathway.

By calculating the inverse Laplace transform of model (13), we obtained the characteristic equation for the Dirac perturbation:

$$y_{bD}(t) = HeavisideTheta[t - T_{zr}]$$
$$k_{mp}k_{mz}\left(\frac{e^{\frac{-t-T_{zr}}{T_{mz}}}}{T_{mz}-T_z} - \frac{e^{\frac{-t-T_{zr}}{T_z}}}{T_{mz}-T_z}\right) \quad (15)$$

By analogy calculating the inverse Laplace transform of the model (14), the characteristic equation for the Heaviside disturbance function was obtained:

$$y_{bH}(t) = HeavisideTheta[t - T_{zr}]$$
$$k_{mp}k_{mz}\left(1 - \frac{e^{\frac{-t-T_{zr}}{T_{mz}}}T_{mz}}{T_{mz}-T_z} + \frac{e^{\frac{-t-T_{zr}}{T_z}}T_z}{T_{mz}-T_z}\right) \quad (16)$$

The resulting Equations 15 and 16, given with negative feedback for the main path of the diagram, limit the light flux passing through the pupil. Together with the main path, they will form a model control system for the visual process, taking into account the system's protection from the effects of image brightness.

The signal conduction velocity in nerve fibers is not high. Moreover, the path length within the visual system is also not long. A delay time T_{zr} can be assumed in the range of 0.002÷0.03 s. The gain coefficients, similar to those in the main path, have values: k_{mp}=1, k_{mz}=1. The time constant values were substituted as follows: T_z=0.08 s, T_{mz}=0.04 s, T_{zr}=0.03 s.

After substituting the values of these parameters for the comparison of the characteristic under disturbance by the Dirac function (15), the characteristic was obtained:

$$y_{bD}(t) = \begin{pmatrix} -25.e^{-25.(-0.03+t)} \\ +25.e^{-12.5(-0.03+t)} \end{pmatrix} HeavisideTheta[-0.03 + t] \quad (17)$$

The time graph of the output function of the pupillary neuromotor coupling path under the disturbance of the Dirac function $y_{bD}(t)$ (17) is shown in Figure 5.

The dynamic waveform of the $y_{bD}(t)$ function is the classical response of a second-order inertial object with a transport delay to a pulse signal. The modeled dynamic waveform of the feedback path output signal is shifted by the transport delay time T_{zr}=0.03 s, has a large dynamic gain of approximately 6 and an exponential decay (derivative action of order 2). The signal settling time is approximately 0.3 s. The plotted waveform determined from equation (17) has a true, natural time history.

Similarly, after substituting the parameter values (T_z=0.08 s, T_{mz}=0.04 s, T_{zr}=0.03 s, k_{mp}=1, k_{mz}=1) into the Heaviside disturbance characteristic equation (16), the following characteristic is obtained:

$$y_{bH}(t) = \begin{pmatrix} 1 + 1.e^{-25.(-0.03+t)} \\ -2.e^{-12.5(-0.03+t)} \end{pmatrix} HeavisideTheta[-0.03 + t] \quad (18)$$

The time graph of the output function of the pupillary neuromotor coupling path $y_{bH}(t)$ (18) with the Heaviside function perturbation is shown in Figure 6.

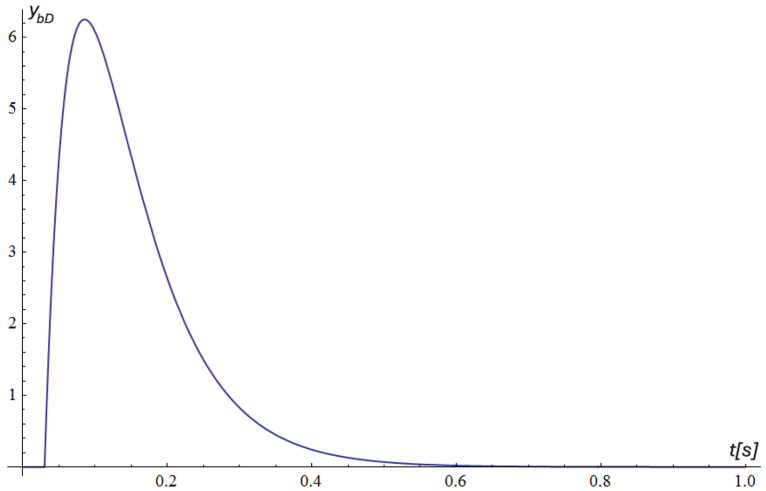

Figure 5. Time graph of the output function of the pupillary neuromotor coupling path $y_{bD}(t)$ with the Dirac function perturbation

The dynamic characteristic $y_{bH}(t)$ shown in Figure 6 is the time course of the output signal of the feedback path related to image brightness. It represents the response to an introduced disturbance in the form of a Heaviside function. The graph is shifted by the transport delay time T_{zr}=0.03 s and has a second-order inertia curve. The signal settling time is approximately 0.3 s. The signal settling at a maximum value of 1 corresponds to the assumed gain coefficient values of 1.

It should be noted that this path does not exist independently in the visual neuromotor system. It is used as a feedback loop for the main visual processing path.

The control system, whose input signal is a light flux that disturbs (irritates) the human visual system, connected to the negative feedback loop of the pupil's neuromotor system associated with the pupillary muscles (image brightness signal), is shown in Figure 2.

The protective mechanism reducing the light flux transmitted to the eye in Figure 2 was modeled as a general equation:

$$G_{mb}(s) = \frac{G_m(s)}{1 + G_m(s)G_b(s)} \tag{19}$$

Taking into account the equations of the model with feedback (19) and the equations of its component models of the main path (5) and the feedback path (11), the Equation 20 was obtained, which is an algebraic model of the main vision path system with one feedback of the neuromotor system of the pupil:

$$G_{mb}(s) = \frac{\dfrac{k_w e^{-T_w s} k_d e^{-T_d s} k_c}{\dfrac{(T_2 s + 1)e^{-T_r s} k_r}{T_1 s + 1}}}{1 + \dfrac{k_w e^{-T_w s} k_d e^{-T_d s} k_c}{\dfrac{(T_2 s + 1)e^{-T_r s} k_r}{T_1 s + 1}} k_{mp} \dfrac{e^{-T_{zr} s}}{T_z s + 1} k_{mz} \dfrac{1}{T_{mz} s + 1}} \tag{20}$$

Equation 20 is a mathematical model in the form of the operator transfer function of a control system with negative image brightness feedback selected for analysis. The choice of only one image brightness feedback signal for system analysis was dictated, among other reasons, by the need to simplify the model for a specific dynamic analysis of the output signal waveform. Despite this simplification, the model is very complex and solving it is a difficult task. The remaining feedback paths will be analyzed simultaneously in the next stage of work on this topic.

From the automation perspective, the presented model is a model of a tracking control system. It does not have a specific setpoint, nor does it contain a component defining the expected shape and range of variation of the irritating light waveform. The human brain takes over the controller's function. It does not have an integral effect, meaning it does not adjust itself through a gradual increase in the generated signal. It operates very quickly, impulsively, and through a derivative, exponential effect, generates a protective signal in the feedback loop. The

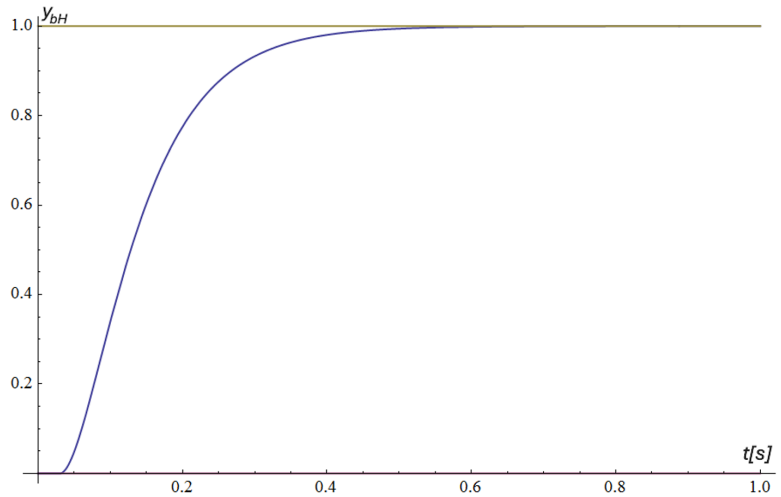

Figure 6. Time graph of the output function of the pupillary neuromotor coupling path $y_{bH}(t)$ with the Heaviside function disturbance

action associated with the generation of the light response signal with this protective coupling can be considered a real proportional-derivative action with inertia.

In the case of a disturbance in the form of the Dirac function (1), the transform of the signal X(s) (3) was used to solve the system, obtaining the equation for the transform of the output signal $Y_{mbD}(s)$:

$$Y_{mbD}(s) = G_{mb}(s)X(s) = \frac{\frac{k_w e^{-T_w s} k_d e^{-T_d s} k_c \frac{(T_2 s+1)e^{-T_r s}k_r}{T_1 s+1}}{1 + \frac{k_w e^{-T_w s} k_d e^{-T_d s} k_c}{1} \frac{(T_2 s+1)e^{-T_r s}k_r}{T_1 s+1} k_{mp} \frac{e^{-T_{zr} s}}{T_z s+1} k_{mz} \frac{1}{T_{mz} s+1}}} \quad (21)$$

In the case of a disturbance in the form of the Heaviside function (2), the transform of the signal X(s) (4) was used to solve the system. The equation of the transform of the output signal was then obtained $Y_{mbH}(s)$:

$$Y_{mbH}(s) = G_{mb}(s)X(s) = \frac{\frac{k_w e^{-T_w s} k_d e^{-T_d s} k_c \frac{(T_2 s+1)e^{-T_r s}k_r}{T_1 s+1}}{1 + \frac{k_w e^{-T_w s} k_d e^{-T_d s} k_c}{1} \frac{(T_2 s+1)e^{-T_r s}k_r}{T_1 s+1} k_{mp} \frac{e^{-T_{zr} s}}{T_z s+1} k_{mz} \frac{1}{T_{mz} s+1}} \frac{1}{s}} \quad (22)$$

The output signal transform for the Dirac function (21) and Heaviside function (22) interferences includes terms describing the transport delays of the current signals. These parameters are present in the main path and also in the analyzed feedback path of the model presented in the block diagram (Figure 2). The transport delay times are very small, ranging from a few hundredths to several ten-thousandths of a second.

After introducing this assumption into Equations 21, 22, the inverse Laplace transform yielded the output signal waveforms $y_{mbD}(t)$ and $y_{mbH}(t)$ in symbolic form. The equations of the output signals $y_{mbD}(t)$ and $y_{mbH}(t)$ determined in the Mathematica program in symbolic form take up several pages and are too extensive to be included in this work.

As with the analysis of the main diagram path and the pupillary neuromotor feedback path, the values of the gain parameters and inertia time constants will be identical, appropriately selected from the range of variability in the first part of the study (k_w=1, k_d=1, k_c=1, k_r=1, T_2=0.0001, T_1=0.05, k_{mp}=1, k_{mz}=1, T_z=0.08, T_{mz}=0.04). Taking into account the adopted assumptions (T_w=0, T_d=0, T_r=0, and T_{zr}=0), the dynamic equations $y_{mbD}(t)$ (23) and $y_{mbH}(t)$ (24) were determined, which were used to plot the time courses of the output signals $y_{mbD}(t)$ and $y_{mbH}(t)$.

When analyzing the assumptions regarding the parameters of the adopted model, one of the fundamental principles of electrical circuit analysis, namely Kirchhoff's first law (current), can be considered for the amplification coefficients. This justifies assuming the coefficient values in the model are equal to 1. This means that, when treating the path element as a node, the microcurrent intensities at the inflow and outflow are equal in magnitude. For the assumptions regarding transport delay times, setting the values to zero applied only to the feedback path. This allowed for a significant simplification of the calculation process without significantly altering the nature of the obtained results.

By substituting the adopted parameters into the signal transform (21) for the Dirac disturbance function, the parameterized equation of the dynamic output signal waveform was obtained in the Mathematica program $y_{mbD}(t)$:

$$y_{mbD}(t) = 6.45204e^{-38.2495t} + e^{(-9.62527-15.3022i)t} \left(\begin{matrix} (6.75398 - 0.731805i) + \\ (6.75398 + 0.731805i)e^{(0.+30.6043i)t} \end{matrix} \right) + 0.002 DiracDelta[t] \quad (23)$$

The time graph of the output function of the main path with feedback of the pupillary neuromotor system for the disturbance with the Dirac function $y_{mbD}(t)$ (23) is shown in Figure 7.

Figure 7 presents the dynamic response of the tracking control system for the eye's reaction to a light stimulus as a Dirac function, taking into account the protective effect of image brightness parameters. As a result of the assumed transport delay values at 0, a waveform originating directly

at the origin was obtained. A very strong brain response occurred in the form of a strongly amplified response signal, which quickly decreased due to the reduction in light flux associated with the pupil size reduction. This rapid derivative action led to an overshoot of the brain's output signal. The model overshoot from the obtained graph is approximately 12%. The output signal has an oscillatory character with a logarithmic damping decrement of approximately d@3.2, indicating very strong damping. The settling time (settling time) is approximately 0.25 s. The eye's reaction to the irritating impulse in the control system disappeared after approximately 0.4 s.

In the case of disturbance with the Heaviside function and substituting the parameter values (identical to the relation (21) for the signal transform (22), the equation of the parameterized dynamic course of the output signal was obtained in the Mathematica program $y_{mbH}(t)$:

$$y_{mbH}(t) = 0.5 - 0.168683e^{-38.2495t} + \\ + e^{(-9.62527-15.3022i)t} \\ \begin{pmatrix} (-0.164658 + 0.337802i) \\ -(0.164658 + 0.337802i) \\ e^{(0.+30.6043i)t} \end{pmatrix} \tag{24}$$

The time course of the output function of the main path with feedback of the pupillary neuromotor system for the disturbance by the Heaviside function $y_{mbH}(t)$ (24) is shown in Figure 8.

The characteristic shown in Figure 8 is the response of the analyzed control system to a

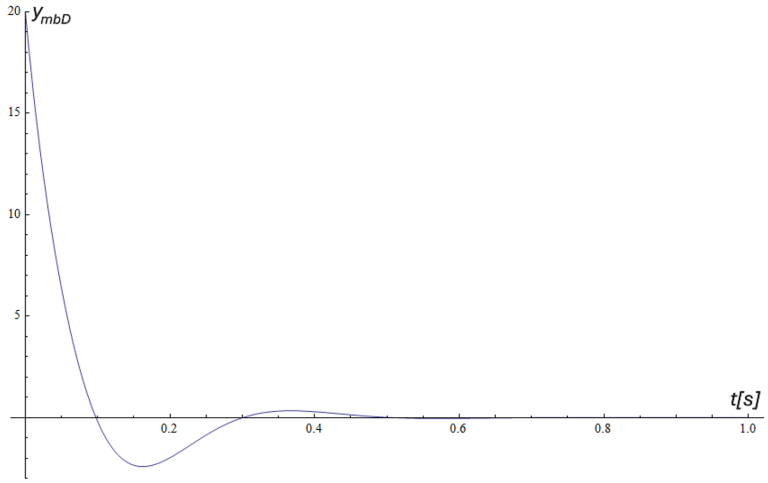

Figure 7. Time course of the output function of the main path with feedback of the pupil's neuromotor system for the disturbance with the Dirac function $y_{mbD}(t)$

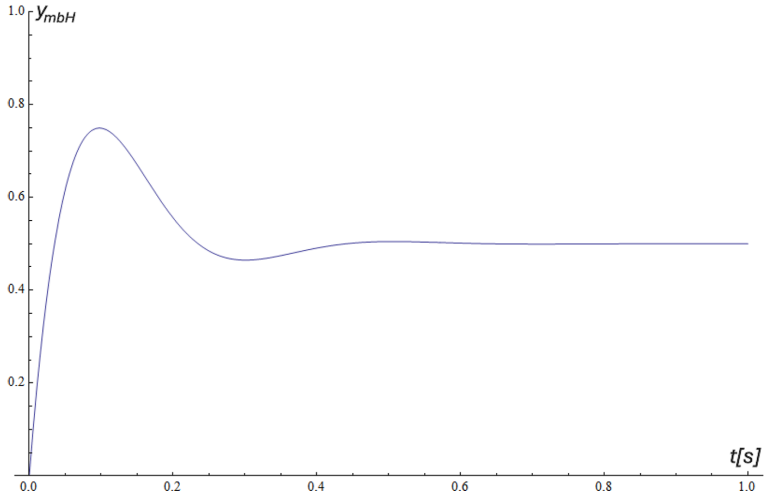

Figure 8. Time course of the output function of the main path with feedback of the pupillary neuromotor system for the disturbance of the Heaviside function $y_{mbH}(t)$

disturbance in the form of a Heaviside function. As a result of assuming zero transport delay times, the waveform begins at the origin of the system. The characteristic has an oscillatory waveform with a logarithmic damping decrement of approximately d@3.6. The model overshoot of the waveform is approximately 25%. The response is the result of a continuous, a moderate_eye irritant, elicited by the brain during a rapid protective response. The waveform settling time is approximately 0.25 s. The steady-state response to such a disturbance is reduced by 50% compared to the waveform without protective feedback, even though the eye is still exposed to the irritating disturbance.

CONCLUSIONS

In this paper, the proposed solutions for an innovative model of human vision were obtained in the form of symbolic equations for the dynamic waveforms of output signals describing the response to light interference. After inserting the model parameter values, the time courses of the determined responses were graphically plotted. The solutions obtained in this work demonstrate a strong dependence on the type of interference, significantly influencing the course and level of response in the human visual process.

Significant parameters were determined from the obtained time histories, which can be used for comparative evaluation in future analyses. The determined values characterizing the waveform with a Dirac function disturbance are as follows: oscillatory waveform, logarithmic damping decrement d_D=3.2, overshoot of approximately 12%, and settling time T_{uD}=0.25 s. For a Heaviside function disturbance: oscillatory waveform with a logarithmic damping coefficient d_H=3.6, overshoot of approximately 25%, and settling time T_{uH}=0.35 s. Important information from the description is the oscillatory waveform with a large logarithmic damping coefficient for both disturbances.

The contemporary development and ubiquity of automated systems compels human work to be fully integrated into this collaboration. In such systems, humans often utilize their sense of sight as a necessary element of the system. In the systems analyzed, humans sometimes act as objects and often as controllers. The systems modeled in this article and the results obtained can be used in the design of mechatronic systems.

The proposed model and its solutions enable an assessment of the capabilities and accuracy of automated systems' interaction with human vision at an initial numerical level. This can provide a basis for potential corrections to the proposed automated system.

An example of such a solution is the advanced medical system in the form of the da Vinci surgical robot. The robot is not autonomous, performing no independent movements; it is fully controlled by a surgeon seated at a console remote from the patient. The interaction of both elements is linked, among other things, by the sense of sight and all the properties of inertial delays in the operation of the elements comprising the modeled system. The 3D vision system allows for the differentiation of tissues, anatomical structures, and nerves.

The use of the human visual sense as an object is encountered in the analysis of athletes' starting systems when assessing false starts. The system detects an athlete's overly rapid reaction, taking into account their inertia in sensing the starting signal. In false start systems, this time is approximately several hundredths of a second. This value is similar to the results presented in this article. Therefore, the modeling and resulting solutions can be used in the design of similar systems. A similar situation occurs in automated systems in aviation, automotive and manufacturing processes.

A supplementary conclusion from the analysis of the obtained solutions is the definition of the next stages of work on the topic of modeling and studying the human vision process. A research plan has been developed to continue the work, expanding the model to include further feedback from other defensive actions of the human vision process, including the reactions of the upper eyelid, facial muscles related to the movement of the lower eyelid, and the movement of muscles that change the focal length of the lens (e.g., the cornea). Simultaneously, laboratory experiments are planned to experimentally identify the values of the temporal parameters adopted in the model.

REFERENCES

1. Daley, W. D., et al. Machine vision algorithm generation using human visual models. In: Precision Agriculture and Biological Quality. SPIE, 1999; 65–72.

2. Thomas, C. W., Gilmore, G. C., Royer, F. L. Models of contrast sensitivity in human vision. IEEE transactions on systems, man, and cybernetics, 1993, 23(3): 857–864.
3. Matsui, T. Theoretical reproduction of spatial frequency characteristics for reaction time based on a spatiotemporal human vision model with accommodative dynamics. Electronics and Communications in Japan (Part III: Fundamental Electronic Science), 1999, 82.7: 39–50.
4. Karmakar, S. et al. Application of digital human modeling and simulation for vision analysis of pilots in a jet aircraft: a case study. Work, 2012, 41.Supplement 1: 3412–3418.
5. Oliver, N. M., Rosario, B., Pentland, A. P. A Bayesian computer vision system for modeling human interactions. IEEE transactions on pattern analysis and machine intelligence, 2000, 22(8): 831–843.
6. Samma, H., Sama, A. S. B. Optimized deep learning vision system for human action recognition from drone images. Multimedia Tools and Applications, 2024, 83(1): 1143–1164.
7. Velesaca, H. O., Vulgarin, J., Vintimilla, B. X. Deep learning-based human height estimation from a stereo vision system. In: 2023 IEEE 13th International Conference on Pattern Recognition Systems (ICPRS). IEEE, 2023; 1–7.
8. Al-Rashdi, M., et al. Light driven visual inspection system for human vision. In: IEEE International Instrumentation and Measurement Technology Conference (I2MTC). IEEE, 2023; 1–6.
9. Wu, Y., et al. A spiking artificial vision architecture based on fully emulating the human vision. Advanced Materials, 2024, 36(19): 2312094.
10. Yalman, Yildiray; Ertürk, Ismail. A new color image quality measure based on YUV transformation and PSNR for human vision system. Turkish Journal of Electrical Engineering and Computer Sciences, 2013, 21(2): 603–612.
11. Hoshino, S., Niimura, K. Robot vision system for human detection and action recognition. Journal of Advanced Computational Intelligence and Intelligent Informatics, 2020, 24(3): 346–356.
12. Ren, Y. Intelligent vehicle violation detection system under human–computer interaction and computer vision. International Journal of Computational Intelligence Systems, 2024, 17(1): 40.
13. Lee, S., et al. Spectral analysis on color detection sharpness of animal vision toward polychromatic vision system. Advanced Materials Technologies, 2025, 10(3): 2400671.
14. Hoshino, S., Niimura, K. Robot vision system for real-time human detection and action recognition. In: International Conference on Intelligent Autonomous Systems. Cham: Springer International Publishing, 2018; 507–519.
15. Csoba, István; Kunkli, Roland. Rendering algorithms for aberrated human vision simulation. Visual Computing for Industry, Biomedicine, and Art, 2023, 6(1): 5.
16. Bochen A., Ambrożkiewicz, B. The influence of light intensity on the operation of vision system in collaborative robot. Advances in Science and Technology. Research Journal, 2023, 17(4).
17. KE, Xianxin, et al. Vision system of facial robot SHFR-III for human-robot interaction. In: International Conference on Informatics in Control, Automation and Robotics. SCITEPRESS, 2016; 472–478.
18. Oda N., Tanaka S. System development of biped robot control coordinated by human vision and head motion. In: 2018 IEEE 15th International Workshop on Advanced Motion Control (AMC). IEEE, 2018. p. 364-369.
19. Makris, S., Aivaliotis, P. AI-based vision system for collision detection in HRC applications. Procedia CIRP, 2022, 106: 156–161.
20. Pladere, T., et al. Inclusivity in stereoscopic XR: Human vision first. Frontiers in Virtual Reality, 2022, 3: 1006021.
21. Yasui, K., et al. One-to-one audio guidance system using human vision, designed for a guide robot. In: 2015 International Conference on Computational Science and Computational Intelligence (CSCI). IEEE, 2015; 841–842.
22. Branson, Steve, et al. The ignorant led by the blind: A hybrid human–machine vision system for fine-grained categorization. International Journal of Computer Vision, 2014, 108.1: 3-29.
23. Piroddi, R., Petrou, M. Integrating human and machine perception to reverse-engineer the human vision system. In: Human And Machine Perception: Communication, Interaction, and Integration. 2005; 119–129.
24. Nowosielski, A., et al. Embedded night-vision system for pedestrian detection. IEEE Sensors Journal, 2020, 20(16): 9293–9304.
25. Kang, C., et al. Development of a peripheral–central vision system for small unmanned aircraft tracking. Journal of Aerospace Information Systems, 2021, 18(9): 645–658.
26. Wang, X., Van De Weem, J., Jonker, P. An advanced active vision system imitating human eye movements. In: 2013 16th International Conference on Advanced Robotics (ICAR). IEEE, 2013; 1–6.
27. Tran, P. V., Le, T. X. Approaching human vision perception to designing visual graph in data visualization. Concurrency and Computation: Practice and Experience, 2021, 33(2): e5722.

28. Deng, W., et al. Learning by doing: A dual-loop implementation architecture of deep active learning and human-machine collaboration for smart robot vision. Robotics and Computer-Integrated Manufacturing, 2024, 86: 102673.
29. Gong, Y., et al. Integrated bionic human retina process and in-sensor RC system based on 2D retinomorphic memristor array. Advanced Functional Materials, 2024, 34(42): 2406547.
30. Katsampiris-Salgado, K., et al. An approach of automated assembly evaluation using AI-based computer vision methods for human–robot collaboration. In: European Robotics Forum. Cham: Springer Nature Switzerland, 2024, 336–340.
31. Al-Rashdi, Mohammed, et al. Light Driven Visual Inspection System for Human Vision. In: 2023 IEEE International Instrumentation and Measurement Technology Conference (I2MTC). IEEE, 2023, 1–6.
32. Antoniewicz J., Zasady automatyki (Automation principles). Wydawnictwa Naukowo-Techniczne, Warszawa 1965 (in Polish).
33. Szczebiot R., Kaczynski R., Goldyn L., Human vision as a multi-circuit mathematical model of the automated control system, Dec 1 2024, Acta Mechanica Et Automatica, 18(4), 161–165.
34. Wolfram, https://www.wolfram.com/mathematica/